2015

Epitaxially Grown Collagen Fibrils Reveal Diversity in Contact Guidance Behavior among Cancer Cells

Juan Wang
Iowa State University, juanw@iastate.edu

Joseph W. Petefish
Iowa State University, petefish@iastate.edu

Andrew C. Hillier
Iowa State University, hillier@iastate.edu

See next page for additional authors

Langmuir

Article

pubs.acs.org/Langmuir

Epitaxially Grown Collagen Fibrils Reveal Diversity in Contact Guidance Behavior among Cancer Cells

Juan Wang,[†] Joseph W. Petefish,[†] Andrew C. Hillier,[†] and Ian C. Schneider*[,†,‡]

[†]Department of Chemical and Biological Engineering and [‡]Department of Genetics, Development and Cell Biology, Iowa State University, Ames, Iowa 50011-2230, United States

Supporting Information

ABSTRACT: Invasion of cancer cells into the surrounding tissue is an important step during cancer progression and is driven by cell migration. Cell migration can be random, but often it is directed by various cues such as aligned fibers composed of extracellular matrix (ECM), a process called contact guidance. During contact guidance, aligned fibers bias migration along the long axis of the fibers. These aligned fibers of ECM are commonly composed of type I collagen, an abundant structural protein around tumors. In this paper, we epitaxially grew several different patterns of organized type I collagen on mica and compared the morphology and contact guidance behavior of two invasive breast cancer cell lines (MDA-MB-231 and MTLn3 cells). Others have shown that these cells randomly migrate in qualitatively different ways. MDA-MB-231 cells exert large traction forces, tightly adhere to the ECM, and migrate with spindle-shaped morphology and thus adopt a mesenchymal mode of migration. MTLn3 cells exert small traction forces, loosely adhere to the ECM, and migrate with a more rounded morphology and thus adopt an amoeboid mode of migration. As the degree of alignment of type I collagen fibrils increases, cells become more elongated and engage in more directed contact guidance. MDA-MB-231 cells perceive the directional signal of highly aligned type I collagen fibrils with high fidelity, elongating to large extents and migrating directionally. Interestingly, behavior in MTLn3 cells differs. While highly aligned type I collagen fibril patterns facilitate spreading and random migration of MTLn3 cells, they do not support elongation or directed migration. Thus, different contact guidance cues bias cell migration differently and the fidelity of contact guidance is cell type dependent, suggesting that ECM alignment is a permissive cue for contact guidance, but requires a cell to have certain properties to interpret that cue.

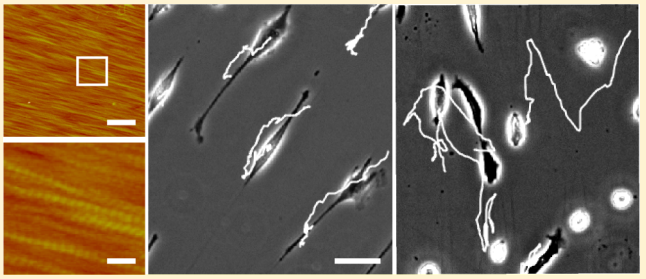

INTRODUCTION

Cell migration is critically important in diverse physiological contexts such as development, immune response, and wound healing, and pathological contexts such as cancer. For example, cell migration allows cancer cells to move away from the tumor, enter and exit blood and lymph vessels, and migrate to secondary tumor sites, in a process called metastasis.[1,2] Metastasis is one of the main causes of mortality in cancer patients and consequently diagnostics aimed at predicting or therapeutic interventions aimed at halting metastasis are attractive. Cell migration can be random, but often it is directed.[3] Directed cell migration allows for more efficient movement toward specific targets. Cues in the extracellular environment that direct migration are numerous and can either cooperate or compete to direct migration.[4] These cues include gradients in growth factors or extracellular matrix (ECM) concentration, mechanical properties, or electric field. Gradients often bias migration toward targets and are thus monodirectional. Aligned fibers composed of ECM also direct cell migration. However, aligned fibers bias migration along their long axis and are thus bidirectional. This type of directed migration is called contact guidance.[5] Contact guidance specifically impacts wound healing,[6] immune response,[7] neuronal development and repair,[8] and cancer metastasis.[9] However, even though cell migration can be directed through several different cues, the fundamental processes carried out during cell migration appear to be conserved.[10]

Cell migration proceeds in steps: protrusion, adhesion, and contraction, which result in traction force generation and tail retraction.[10] In 3D environments the additional step of ECM degradation is usually included.[11] The cell senses contact guidance cues via adhesion between receptors such as integrins and the fibers. Much of this work has been conducted on ridges that mimic ECM fibers showing that contact guidance cues act to align focal adhesions[12−14] and the actin cytoskeleton,[12,13,15,16] resulting in directional migration. Along with focal adhesions and the actin cytoskeleton, the ability of cells to transmit force seems to play a role as decreasing contractility seems to diminish contact guidance fidelity on microcontact printed lines of collagen type I.[17] Migrational steps are organized differently in different cells, resulting in a developing hypothesis that cells adopt different modes of migration.[18]

Received: August 14, 2014
Revised: December 8, 2014
Published: December 8, 2014

DOI: 10.1021/la503254x
Langmuir 2015, 31, 307−314

Single cell modes include the amoeboid, mesenchymal, blebbing,[19] lobopodial,[20] and cytoskeletal independent modes of migration.[21] Of these, the amoeboid and mesenchymal seem to be the best characterized.[18] The amoeboid mode of migration is proteinase independent. These cells are also dependent on myosin contractility to squeeze through pores, but tend to not bind the ECM strongly. The mesenchymal mode of migration is proteinase dependent. These cells are less dependent on myosin contractility as they can degrade matrix to generate larger pores, but tend to bind the matrix more strongly. Whether amoeboid or mesenchymal, cells must still interact with the ECM, even if weakly or nonspecifically. The ECM that surrounds the tumor is often composed of a dense but porous network of entangled and perhaps cross-linked collagen type I.[22]

Collagen type I is a heterotrimer that assembles into fibrils with tightly regulated ultrastructural characteristics such as D-periodic banding.[23] This structure is a hallmark of biologically relevant collagen fibrils and is critical for contact guidance.[24] Collagen fibrils can be aligned and bundled into fibers through contractility mediated mechanisms in some tissues.[25,26] In particular, the tissue surrounding breast tumors appears to undergo a dramatic change, whereby fibers are no longer oriented parallel to the tumor margin, but are oriented perpendicularly to the tumor margin.[9] This facilitates directed migration of cancer cells to the surrounding tissue during invasion and metastasis. Additionally, the density and mechanical properties of collagen ECM has been suggested as a good indicator of future invasion and metastasis.[9,27] Consequently, to better understand fundamental cell biology and design better diagnostic strategies, it is important to understand how cell migration is quantitatively altered in response to collagen fiber characteristics such as degree of alignment, diameter, density, and mechanical properties, as well as among different cells with intrinsically different migrational modes. This requires using systems where collagen fibril (or fiber) characteristics can be altered and assessing cell migration behavior across several different cell lines.

The past 10 years have seen a dramatic increase in the engineering approaches by which to fabricate fiber networks with specific fiber characteristics. In particular, several techniques have emerged to generate aligned fibers or fiber-like entities. These methods include fabricating ridges,[28] electrospinning,[29] fiber drawing,[30] epitaxial growth,[31] micro-contact printing,[32] flow-based alignment,[33,34] and magnetic bead alignment.[35] Surprisingly, these approaches have not been fully utilized to understand contact guidance. Here we focus on the elegant and simple approach of epitaxially growing collagen type I (hereafter referred to as collagen) fibrils on mica to generate fibril structures with different organizational characteristics. Collagen in solution adsorbs to freshly cleaved mica surfaces and assembles into fibrils. Collagen fibril assembly is governed by collagen−collagen and collagen−mica electrostatic interactions.[36,37] The interaction with mica is due in part to potassium ions that remain on the surface after cleavage.[37] Solution phase conditions such as the collagen concentration and incubation time determine fibril size and density,[37−39] the pH of the solution determines fibril density and alignment,[40,41] and the ionic species determine the fibril density, alignment, and presence of D-banding.[41−43] Because potassium ions seem to be important in initiating D-banding, others have examined different potassium ion concentrations, and they appear to regulate fibril size, density, and alignment.[39−41] Finally, muscovite mica orders collagen differently than phlogopite mica.[39,43] The geometry of epitaxially grown collagen fibrils resembles a thin tape as opposed to a cylinder as seen in vivo. However, there are several advantages to this approach over other approaches described above, including the ease in forming a diverse set of structures and efficiency in forming D-bands with similar spacing as those seen in collagen fibrils in vivo. While these substrates have been used to assess the effect of D-banding on fibroblast contact guidance[24] and the coupling of adhesion and proteinase activity,[44] they have not been used to assess contact guidance across different collagen structures and among different cell types.

In this paper, we generated several different organizational patterns of collagen and assessed how cell morphology, orientation, and contact guidance behavior depended on the collagen organization. Highly organized collagen fibrils generated robust contact guidance. Less well organized fibrils induced contact guidance, but to a lesser extent. Disorganized collagen fibrils and physically adsorbed collagen allowed cells to spread, but did not direct migration. We examined this behavior in two different breast cancer cell types and found profound differences. MDA-MB-231 cells which migrate with a mesenchymal mode of migration and which exert high traction force were highly directional, but MTLn3 cells which migrate with an amoeboid mode of migration and which exert lower traction force were not directional at all, even though they spread and migrated well on the aligned fibrils. This demonstrates that different contact guidance cues can bias cell migration differently and the fidelity of contact guidance is highly dependent on cell type, suggesting that the ECM alignment is a permissive cue for contact guidance, but requires a cell to have certain properties in order to interpret that cue. Collagen fibrils assembled on mica offer an interesting platform on which to exquisitely tune contact guidance signals and examine cellular responses at the level of migration.

EXPERIMENTAL SECTION

Reagents and Cells. A rat mammary basal[45] adenocarcinoma cell line (MTLn3, Jeffrey E. Segall, Albert Einstein College of Medicine) was maintained in subculturing media at 37 °C in 5% CO_2. Subculturing media for MTLn3 cells was MEMα (Life Technologies, Grand Island, NY, USA) containing 5% fetal bovine serum (Life Technologies) and 1% penicillin−streptomycin (Life Technologies). A human mammary basal/claudin low[46] carcinoma cell line (MDA-MB-231, ATCC, Manassas, VA, USA) was maintained in cell culture media at 37 °C in 5% CO_2. Subculturing media for MDA-MB-231 cells was DMEM (Life Technologies) containing 10% fetal bovine serum (Life Technologies) and 1% penicillin−streptomycin (Life Technologies). Imaging media was the same as the subculturing media, with the exception that no phenol red was included and that 12 mM HEPES (Sigma-Aldrich, St. Louis, MO, USA) was included. High concentration non-pepsin-treated rat tail collagen type I (BD Bioscience, Hampton, New Hampshire, USA) was used.

Collagen Substrate Treatment. Freshly and uniformly cleaving mica is a required step in assembling reproducible collagen fibril fields. A 15 mm × 15 mm piece of muscovite mica (highest grade VI, Ted Pella, Redding, CA, USA) was freshly cleaved using tape. A flat layer of the mica that remained on the tape was discarded. Collagen type I was diluted in the buffer solution to the proper concentration and the buffer solution was incubated on the mica at room temperature. After incubation the collagen solution was washed with distilled water, the mica was laid against the edge of a tissue culture dish, and the mica was allowed to dry overnight and used the next day. There were four different buffer solutions. Buffer solution 1 consisted of 50 mM Tris-HCl (Fisher Scientific, Hampton, New Hampshire, USA) and 200 mM KCl (Fisher Scientific) at pH 9.2. Buffer solution 2 consisted of 50

DOI: 10.1021/la503254x
Langmuir 2015, 31, 307−314

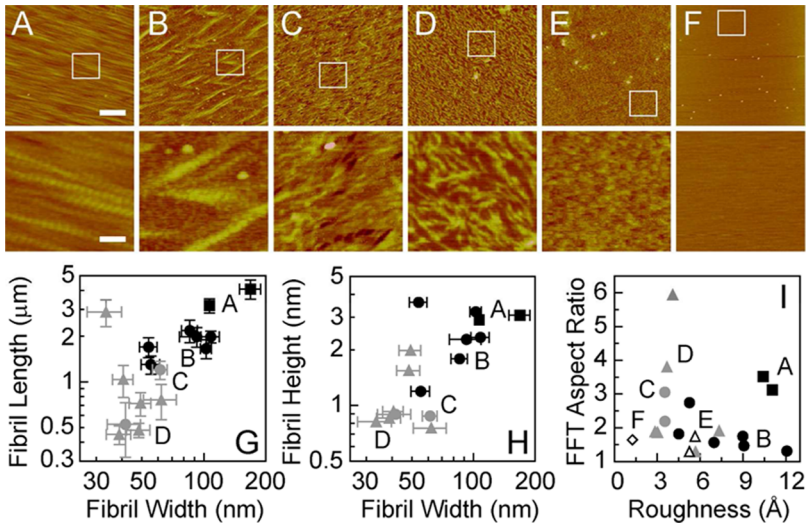

Figure 1. Characterization of collagen organization on freshly cleaved mica using atomic force microscopy (AFM) under six conditions: (A) pH 9.2, 200 mM KCl, 10 μg/mL collagen, 1.5 h incubation time; (B) pH 7.5, 200 mM KCl, 100 μg/mL collagen, 3 h incubation time; (C) pH 7.5, 200 mM KCl, 100 μg/mL collagen, 20 min incubation time; (D) pH 4.3, 200 mM KCl, 10 μg/mL collagen, 20 min incubation time; (E) pH 4.2, 0 mM KCl, 100 μg/mL collagen, 3 h incubation time; and (F) bare mica. Top: 5 μm × 5 μm scan (calibration bar length = 1 μm). Bottom: 1 μm × 1 μm enlarged region outlined in the square above (calibration bar length = 200 nm). (G) Fibril length and width. (H) Fibril height and width. Each data point was generated from a sample image from one independent collagen deposition experiment. Error bars are 95% confidence intervals for fibril length and width were determined from measuring >10 fibrils per image. (I) FFT aspect ratio and surface roughness. A: black squares, B: black circles, C: gray circles, D: gray triangles, E: open triangles, and F: open diamond.

mM Tris-HCl and 200 mM KCl at pH 7.5. Buffer solution 3 consisted of 50 mM citric acid-sodium citrate (Fisher Scientific) and 200 mM KCl at pH 4.3. Buffer solution 4 consisted of 50 mM citric acid-sodium citrate and 0 mM KCl at pH 4.2.

Atomic Force Microscope (AFM) Imaging and Analysis. A Dimension 3100 scanning probe microscope with Nanoscope IV controller (Veeco Metrology, LLC, Santa Barbara, CA) was utilized to obtain height images of collagen fibrils on mica. Imaging was conducted in tapping mode using silicon TESP7 AFM tips (Veeco Metrology, LLC, Santa Barbara, CA) with a spring constant of ~79 N/m and resonance frequency of ~269 kHz. Roughness of type I collagen fibrils was calculated by computing the standard deviation of the height over a 5 μm × 5 μm scan area. Fast Fourier transform (FFT) aspect ratio processing steps are shown in Supporting Information Figure 1 and all steps were carried out in ImageJ. An image representing the FFT was computed in ImageJ. This FFT operation translates spatial information into frequency information and is thus useful in quantifying repeating patterns and length scales. This FFT image was binarized based on a threshold that was two standard deviations higher than the FFT image average, resulting in a shape centered at the origin. Several serial image processing steps were conducted in ImageJ in order to eliminate small objects and fill holes in the dominant shape centered at the origin. The following processing steps were used in order: fill holes (4 connected background elements), erode, dilate, open, and close (structured element for erosion, dilation, opening and closing is a 3 × 3 matrix). These were followed by another erode and open function. Finally, an ellipse was fit to the zero order signal using the analyze particles function in ImageJ, which was always the largest continuous shape. The aspect ratio was defined as the long axis divided by the short axis of the ellipse. Fibril height was calculated by fitting the height distribution with a Gaussian function and determining the peak width at 30% of the maximum height. Under this criterion the thickness of the unpolymerized collagen was roughly 1.5 nm, which matches well with the known diameter of the collagen heterotrimer. Fibril height could not be unambiguously determined given the high density of the fibril fields and some uncertainty as to whether the AFM tip could at times penetrate to the mica layer below. Fibril width and length were measured manually using ImageJ. While there is high confidence in fibril width, fibril length is a bit more difficult to measure given some ambiguity in where fibrils start and stop.

Live Cell Imaging. MDA-MB-231 cells were incubated for 1 h and MTLn3 cells were incubated for 12 h on organized type I collagen substrates in imaging media. Mica with type I collagen fibrils and cells attached to the fibrils were inverted onto two strips of double-sided tape attached to a microscope slide to generate a flow chamber. The chamber was filled with imaging media and sealed with VALAP. Chambers were imaged by phase contrast microscopy on a heated stage at 37 °C every 2 min for 12 h. Images were captured at 10× (NA 0.50, Nikon) with a charge-coupled device (CoolSNAP HQ2, Photometrics) attached to an inverted microscope (Ti-E, Nikon) that was driven by μManager.[47] Cell centroids were identified and tracked manually using the MTrackJ plugins of ImageJ. Cell speed and directionality were calculated over a time lag of 2 min averaged over 12 h as described in a previous paper.[17]

Immunofluorescence Imaging. MDA-MB-231 cells were incubated for 4 h and MTLn3 cells were incubated for 12 h on organized type I collagen, fixed with 4% paraformaldehyde, permeabilized with 0.5% Triton-X, and stained for F-actin, a cytoskeletal protein and paxillin, an adhesion protein. F-actin was stained using Alexa 488-phalloidin (Life Technologies) and paxillin was stained using mouse-anti-paxillin antibody (349, BD Biosciences) and a donkey-anti-mouse Cy3 antibody (Jackson Immuno Research). Fixed and stained cells were imaged by epifluorescence using a 60× oil objective (NA 1.49, Nikon) on the same microscope as described above. Aspect ratio for each cell was calculated by dividing the length of each cell by its width. Orientation was only calculated for cells with an aspect ratio ≥1.3.

Calculating and Fitting Cell Orientation Distributions. Of the cells that were adequately elongated (aspect ratio ≥1.3), the orientation direction was calculated along the long axis of the cell. Orientation distributions across experimental replicates over several days were aligned and the dominant peak was set at 30°, given that the fibril orientation and cell orientation were not readily imaged simultaneously. Furthermore, orientation distributions were fitted by double Gaussians governed by the following equation:

DOI: 10.1021/la503254x
Langmuir 2015, 31, 307−314

$$f = a_1\left(\exp\left[\frac{-(\theta-30)^2}{2b_1^2}\right] + \exp\left[\frac{-(\theta-210)^2}{2b_1^2}\right]\right) + a_2\left(\exp\left[\frac{-(\theta-90)^2}{2b_2^2}\right] + \exp\left[\frac{-(\theta+90)^2}{2b_2^2}\right]\right) \quad (1)$$

where f is the frequency fraction and θ is the orientation angle in deg. The second and fourth term arise in order to ensure that the Gaussian is propagated periodically. For wide distributions (large b_1 and b_2), the left tail of the Gaussian at 30° contributes to fractions around 180° and the right tail of the Gaussian at 90° contributes to fractions around 0°. Confidence intervals of 95% were calculated using the nlparci function in Matlab (Mathworks), which uses the fitting residuals and the Jacobian of the fitting equation to estimate the 95% confidence intervals on fitting parameters. A peak was assigned only if the confidence interval of a_1 or a_2 was greater than zero and if that of b_1 or b_2 was less than 30°. Wide distributions are less likely to be peaks. If either of these criteria was not achieved, fits to either a single Gaussian (terms 1 and 2 of eq 1) or a constant value were used.

RESULTS AND DISCUSSION

Characterization of Collagen Organization on Mica. Determining the contact guidance fidelity of migrating cells requires tight control over the organization of the ECM. It is well-established that collagen fibrils epitaxially grow on mica surfaces. Furthermore, the fibril characteristics can be controlled by solution phase properties such as pH, ionic strength, ion species, incubation time, and collagen concentration. In this paper, we characterize collagen organization using atomic force microscopy (AFM) under six conditions (Figure 1A–F). Conditions were chosen to yield a diversity of collagen organizational patterns, including highly aligned fibrils of large width and height (Figure 1A), multidirectional fibrils of intermediate width and height (Figure 1B), poorly aligned fibrils of small width and height (Figure 1C and D), and punctate spots (Figure 1E). In addition, bare mica was also assessed (Figure 1F). As seen previously, solutions with high pH and/or long incubation times/high collagen concentrations produced the largest fibrils (Figure 1G,H; see A and B). Solutions with intermediate to low pH coupled with short incubation times/low collagen concentrations produced smaller fibrils (Figure 1G,H; see C and D). Finally, solutions with low pH with no potassium ions inhibited fibril formation. The degree of fibril alignment was quantified by examining the fast Fourier transform (FFT) of the image and measuring the aspect ratio of the zero order signal after image processing as described in the Experimental section (Supporting Information Figure 1). Randomly organized fields (E and F) or fibril fields with dominant angles that are nearly perpendicular (B) should have an aspect ratio close to 1, and highly aligned fibrils (A) should have a large aspect ratio (Figure 1I). The highly organized, large collagen fibrils show a characteristic D-banding along their length, producing stripes in the FFT oriented perpendicularly to the fibril orientation (Supporting Information Figure 1A). Consequently, the long axis of the high-intensity zero-order signal is perpendicular to the orientation axis of the fibrils. In addition to the FFT aspect ratio, the roughness of the surface was calculated showing that fibrils of larger diameter (A and B) were rougher than the smaller fibrils (C and D), collagen pucta (E), or bare mica (F) (Figure 1I). Comparison of the roughness of condition A with the roughness of condition C, D, or E using a two-tailed, unequal variance Student's t-test yielded p values of less than 0.05. Comparison of the roughness of condition B with the roughness of condition C, D, or E yielded p values of less than 0.05, except for E which yielded a p value of 0.095. Finally, when roughnesses of A and B as well as C and D were grouped together the p values for comparison in roughness between groups AB and CD or E were both less than 0.05. All conditions were at least twice as rough as bare mica. Given this surface characterization of the collagen organization, we were interested in determining cell adhesion and migration behavior on the different collagen organizational patterns.

Breast Cancer Cell Morphology and Migration Behavior on Epitaxially Grown Collagen Fibrils. A well-characterized cell line (MDA-MB-231) was used. These cells adhere and migrate on collagen fibrils, are contractile, and adopt a mesenchymal mode of migration, which is characterized by high proteinase activity coupled with adhesion to the ECM. MDA-MB-231 cells were plated on the six different substrates characterized in Figure 1 and were fixed and stained for both F-actin, a cytoskeletal protein, and paxillin, an adhesion protein. Cells were spread and elongated on the highly aligned fibrils of large width and height (Figure 2A). Cells were spread, but not elongated on other fibril organizations and punctate collagen (Figure 2B–E). Finally, cells did not spread on the bare mica (Figure 2F). High resolution images show that focal adhesions and bundles of F-actin are generated on any substrate with collagen. Aligned collagen fibrils of large width and height result in elongation of both focal adhesions and F-actin bundles (Figure 3). The cell morphology was quantified by calculating an aspect ratio of the cell from the length and width

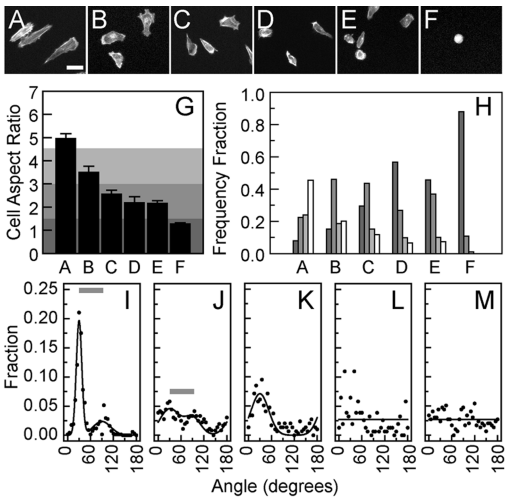

Figure 2. Morphology and orientation of MDA-MB-231 cells under six organized collagen assembly conditions. (A–F) Conditions shown in Figure 1A–F. Representative cells are shown stained for F-actin. Calibration bar length = 30 μm. (G) Cell aspect ratio was calculated for cells by examining F-actin images for conditions shown in Figure 1A–F (A. (N_{days} = 5 and N_{cells} = 909), B. (N_{days} = 3 and N_{cells} = 550), C. (N_{days} = 3 and N_{cells} = 427), D. (N_{days} = 3 and N_{cells} = 316), E. (N_{days} = 3 and N_{cells} = 526), F. (N_{days} = 3 and N_{cells} = 165)). Different gray values indicate arbitrary, evenly spaced cell aspect ratio ranges. Error bars are 95% confidence intervals. H. The frequency fraction of cells within each aspect ratio range denoted with the same gray levels as shown in G and for conditions shown in Figure 1A–F. (I–M) Angle distributions of cells for conditions shown in Figure 1A–F with aspect ratios >1.3 (A. (N_{days} = 4 and N_{cells} = 575), B. (N_{days} = 2 and N_{cells} = 362), C. (N_{days} = 2 and N_{cells} = 294), D. (N_{days} = 2 and N_{cells} = 113), E. (N_{days} = 2 and N_{cells} = 294)). Gray bars correspond to ~60° spacing between peaks 1 and 2.

DOI: 10.1021/la503254x
Langmuir 2015, 31, 307–314

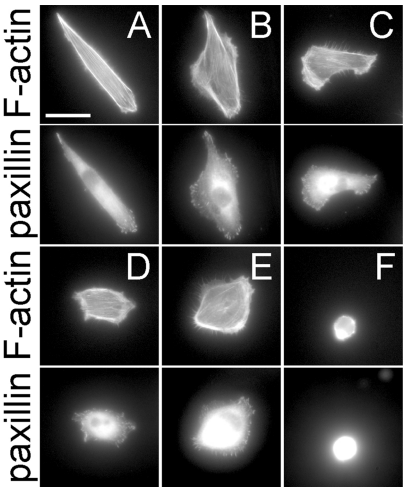

Figure 3. Morphology and protein localization of MDA-MB-231 cells under six differently organized collagen substrates. (A–F) Cells were plated under conditions shown in Figure 1A–F and stained for Top: F-actin and Bottom: a focal adhesion marker, paxillin. Calibration bar length = 30 μm.

measurements and agreed with the qualitative observations (Figure 2G). Cell aspect ratios were divided into groups including cells that were elongated (white), slightly elongated (gray), not elongated, but spread (dark gray), and not spread (darkest gray). The population of cells was not homogeneous, so the fraction of cells in each aspect ratio group was plotted and showed a consistent trend of a shift in the distribution from elongated, spread cells, to unspread cells as the organization of the collagen decreased (A–F) (Figure 2H).

High cell elongation does not necessarily indicate high cell alignment with the fibrils or a high degree of contact guidance, so the orientation distributions of the cells were calculated as well. The highly aligned fibrils of large width and height generated two peaks, which were offset by 60° (Figure 2I). While across one coverslip the alignment direction is fairly homogeneous, other less frequent directions are seen (Figure 4A). This contrasted with the no fibril condition that showed

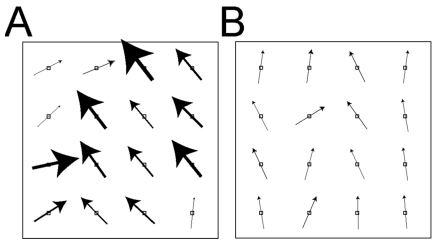

Figure 4. Cell orientation of MDA-MB-231 cells from images taken on different areas of the epitaxially grown collagen for dense monodirectional fibrils (Figure 1A, pH 9.2, 200 mM KCl, 10 μg/mL collagen, 1.5 h incubation time) and no fibrils (Figure 1E, pH 4.2, 0 mM KCl, 100 μg/mL collagen, 3 h incubation). The coverslip is roughly 25 mm × 25 mm and each image field is roughly 0.4 mm × 0.4 mm. The arrow direction indicates the average cell orientation direction in an image field and the arrow weight is inversely proportional to the standard deviation of directions in an image field. A large standard deviation is denoted by a light weight and a small standard deviation is denoted by a heavy weight. For random cell orientation angles, the average orientation is 90° (pointing upward) and the line weight approaches zero.

random alignment (Figure 4B). Mica is hexagonally ordered, leading to a threefold symmetry. However, others have shown that collagen fibril orientation is set by surface charge polarity[37] established by parallel and alternating lines of silicon oxide above and below the surface plane in the [1 1 0] direction.[42] When mica is incompletely cleaved, steps corresponding to a different layer of mica can remain on the surface at some places on the sample. These two different mica layers might have a difference in the orientation direction of these lines of silicon oxide above and below the surface plane, leading to alternative collagen fibril and cell orientations at ±60° over large length scales (~1000 μm). The multidirectional fibrils of large width and height display multiple directions, even on small length scales (~5 μm), so the orientation peaks are much less pronounced (Figure 2J). The other fibril orientations show solitary peaks (Figure 2K) or no peaks at all (Figure 2L). Punctate collagen also shows no peak at all (Figure 2M). We quantified the correlation between either the cell aspect ratio or cell orientation peak height and FFT aspect ratio or surface roughness using the Pearson correlation coefficient. Cell aspect ratio correlated better with surface roughness (r = 0.77) than FFT aspect ratio (r = 0.099). On the other hand, cell orientation peak height correlated slightly better with FFT aspect ratio (r = 0.37) than surface roughness (r = 0.33). These data along with those in Figure 2 indicate that the aligned collagen fibrils of large width and height, and to a lesser extent the multidirectional collagen fibrils of large width and height are best able to generate elongation and orientation in MDA-MB-231 cells, suggesting they are better contact guidance substrates. Given this, we examined the contact guidance fidelity directly by measuring the directionality of MDA-MB-231 cells migrating on these organizational patterns of collagen. MDA-MB-231 cells were plated on substrates shown in Figure 1A and B, imaged over 12 h (Figure 5A) and cell nuclei were

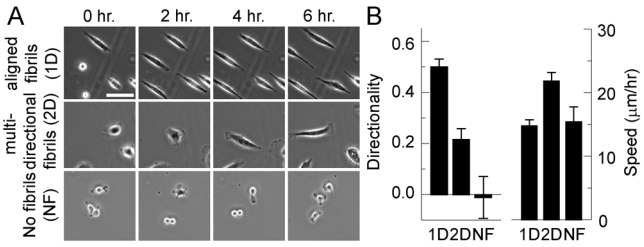

Figure 5. Migration behavior of MDA-MB-231 cells on three different organizational patterns of epitaxially grown collagen: aligned collagen fibrils of large width and height (Figure 1A, pH 9.2, 200 mM KCl, 10 μg/mL collagen, 1.5 h incubation time), multidirectional collagen fibrils of large width and height (Figure 1B, pH 7.5, 200 mM KCl, 100 μg/mL collagen, 3 h incubation time), and unpolymerized collagen (Figure 1E, pH 4.2, 0 mM KCl, 100 μg/mL collagen, 3 h incubation time). (A) Montage of phase contrast images of MDA-MB-231 cells at different timepoints during migration. Calibration bar length = 30 μm. (B) Left: directionality and Right: cell migration speed of MDA-MB-231 cells. $N_{days} \geq 3$ and $N_{cells} \geq 148$. Error bars are 95% confidence intervals.

tracked. Cell directionality was calculated using the following equation:

$$\mathrm{DI} = \frac{1}{N}\sum_{i=1}^{N}\cos(2\theta_i) \qquad (2)$$

DOI: 10.1021/la503254x
Langmuir 2015, 31, 307–314

where N is the number of time intervals contained in an individual cell track and θ_i is the angle of the cell movement with respect to the collagen fibrils. The directionality essentially quantifies the projection of cell displacement along the long axis of the fibrils, thus giving a good representation of the contact guidance fidelity. A directionality of 1 defines a situation where a cell only moves in two directions along the fibril (0° and 180°). A directionality of 0 defines a situation where a cell moves randomly or at a 45° with respect to the fibrils. Finally, a directionality of −1 defines a situation where a cell moves perpendicularly with respect to a fibril (90°). MDA-MB-231 cells show high directionality on aligned collagen fibrils of large width and height and a lower directionality on the multidirectional collagen fibrils of large width and height (Figure 5). MDA-MB-231 cells do not directionally migrate on unpolymerized collagen substrates (Figure 5). Cell migration speed on collagen fibril substrates showed the opposite behavior. Multidirectional collagen organization resulted in high speed, whereas aligned collagen organization resulted in lower speed (Figure 5B). Cell speed on unpolymerized collagen substrates was low and similar to that on the aligned collagen fibrils (Figure 5B). The migrational behavior on collagen fibrils agrees with many studies showing that directional persistence is often inversely dependent on cell migration speed.[48] This suggests that MDA-MB-231 cells are sensitive to aligned collagen fibrils, leading to high fidelity contact guidance. This is important given that in vivo data indicate the presence of aligned collagen fibrils in the tumor microenvironment in breast cancer.

Comparison of Contact Guidance Behavior between Different Breast Cancer Cell Lines. We were interested in whether this contact guidance behavior was universal or restricted to this one cell type, so we performed similar assays using the MTLn3 cell line, another commonly used breast cancer cell line. Both MDA-MB-231 and MTLn3 cells are basal or basal-like cells and adhere and migrate on collagen; however, there are several differences. First, MDA-MB-231 cells adopt more of a mesenchymal mode of migration in 3D environments compared to the amoeboid mode of migration that MTLn3 cells adopt.[49,50] In 2D environments, MTLn3 cells adopt a fan shaped morphology, whereas MDA-MB-231 cells are more spindle-like.[51] Finally, MDA-MB-231 cells exert roughly 10-fold higher traction forces than MTLn3 cells, resulting in more stable focal adhesions and F-actin bundles and slower 2D migrational speeds.[49,52,53] MTLn3 cells generated focal adhesions, assembled F-actin bundles, spread, and migrated on different organizational patterns of collagen (Figures 6 and 7). However, MTLn3 cells did not elongate as readily as MDA-MB-231 cells (Figure 2G and H compared to Figure 6A and B) and showed no peak in cell orientation on highly aligned fibrils (Figure 2I compared Figure 6C). However, two peaks did occur on multidirectional fibrils (Figure 2J compared with Figure 6D). MTLn3 cells migrated more rapidly than MDA-MB-231 cells on aligned fibrils, but slightly more slowly on multidirectional fibrils (Figure 5B compared to Figure 7B). Both were statistically significant ($p < 0.05$). Finally, MTLn3 cells did not interpret the aligned fibrils as a contact guidance cue (Figure 7B). MDA-MB-231 cells had a much higher directionality than MTLn3 cells under both fibril organizational conditions (Figure 5 compared to Figure 7). This is interesting, given that MTLn3 cells migrate directionally on microcontact printed lines of collagen on mica (Supporting Information Figure 2) and glass.[17] Two different surface characteristics

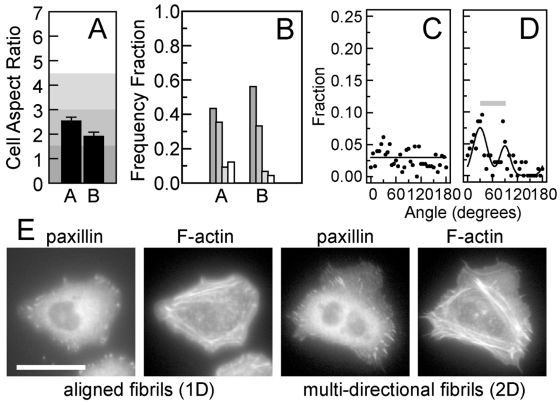

Figure 6. Morphology and orientation of MTLn-3 cells under two organized collagen conditions: aligned collagen fibrils of large width and height (Figure 1A, pH 9.2, 200 mM KCl, 10 μg/mL collagen, 1.5 h incubation time) and multidirectional collagen fibrils of large width and height (Figure 1B, pH 7.5, 200 mM KCl, 100 μg/mL collagen, 3 h incubation time). (A) Cell aspect ratio was calculated for cells by examining F-actin images for conditions shown in Figure 1A and B (A. (N_{days} = 5 and N_{cells} = 940) and B. (N_{days} = 2 and N_{cells} = 242)). Different gray values indicate arbitrary, evenly spaced cell aspect ratio ranges. Error bars are 95% confidence intervals. (B) Frequency fraction of cells within each aspect ratio range denoted with the same gray levels as shown in A. (C,D) Angle distributions of cells on for conditions shown in Figure 1A,B with aspect ratios of >1.3 (A. (N_{days} = 5 and N_{cells} = 468) and B. (N_{days} = 2 and N_{cells} = 94)). The gray bar corresponds to ∼60° spacing between peaks 1 and 2. (E) MTLn3 cells were plated on aligned fibrils of large width and height (Figure 1A, pH 9.2, 200 mM KCl, 10 μg/mL collagen, 1.5 h incubation time) and multidirectional fibrils of large width and height (Figure 1B, pH 7.5, 200 mM KCl, 100 μg/mL collagen, 3 h incubation time) and stained for Left: a focal adhesion marker, paxillin, and Right: F-actin. Calibration length = 30 μm.

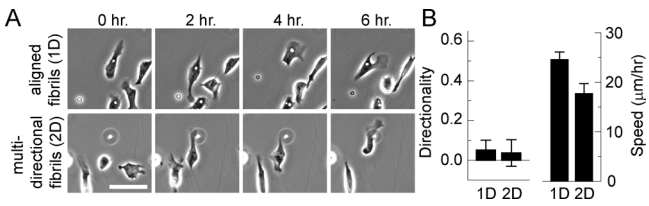

Figure 7. Migration behavior of MTLn3 cells on two different organizational patterns of epitaxially grown collagen: aligned collagen fibrils of large width and height (Figure 1A, pH 9.2, 200 mM KCl, 10 μg/mL collagen, 1.5 h incubation time) and multidirectional collagen fibrils of large width and height (Figure 1B, pH 7.5, 200 mM KCl, 100 μg/mL collagen, 3 h incubation time). (A) Montage of phase contrast images of MTLn3 cells at different time points during migration. Calibration bar length = 30 μm. (B) Left: directionality and Right: cell migration speed of MTLn3 cells. $N_{days} \geq 3$ and $N_{cells} \geq 84$. Error bars are 95% confidence intervals.

could lead to this. First, microcontact printed collagen is heterotrimeric and not assembled into collagen fibrils. It is possible that certain contact guidance sites for MTLn3 cells are masked when collagen assembles into fibrils. Second, the lines of collagen are sparser than the collagen fibrils used here and separated by less adhesive areas. When MTLn3 cells are faced with nonadhesive areas as in the microcontact printed lines, it is possible that this induces the contact guidance.

Several possibilities could explain the difference in contact guidance fidelity between MDA-MB-231 cells and MTLn3 cells. First, it is possible that altering the traction forces exerted

DOI: 10.1021/la503254x
Langmuir 2015, 31, 307−314

by the cells on the substrate might change the directional fidelity. Traction force could act to align focal adhesions, therefore by increasing the traction force in MTLn3 cells, one might make more directional cells and by decreasing the traction force in MDA-MB-231 cells, one might make less directional cells. Second, it is possible that receptor expression could be different among the two cells leading to differences in directional fidelity. These experiments were conducted in serum, where multiple ECM proteins such as fibronectin and vitronectin can bind to the collagen. Perhaps differences in the usage of $\alpha_2\beta_1$ (collagen) integrins vs $\alpha_5\beta_1$ and $\alpha_v\beta_3$ (fibronectin and vitronectin) integrins might mediate this response. Finally, Rho-family signaling has been linked to contact guidance. First, Rho and its downstream myosin light chain kinase, ROCK, are indeed important to contact guidance in 3D collagen matrices. However, this importance is related to the role of Rho and ROCK in collagen reorganization rather than a role in intrinsic ability to sense contact guidance cues. Indeed, inhibiting Rho and ROCK did not inhibit migration into prealigned collagen gels.[25] However, it is possible that Rho and ROCK regulate intrinsic contact guidance differently between 2D and 3D, making it a possible candidate to explain the differences between these cell types. In addition to Rho, Rac activity has been linked to directional migration.[54] Higher Rac activity results in more lateral protrusions and less directionally persistent migrational behaviors, whereas lower Rac activity inhibits lateral protrusions and results in more directionally persistent migrational behaviors. It is possible that Rac activity among the two different cell lines is different. Given that Rac activity differs in 2D and 3D environments, it will be interesting to determine if this difference in contact guidance holds for cells migrating in 3D collagen networks. The finding that different cell types interpret directional cues differently, even though they bind and migrate in response to those cues, might have a dramatic impact on cancer diagnosis. Robust reorganization and radial alignment of the collagen ECM around breast tumors has led others to suggest that these could be used as diagnostic markers. We believe this to be a good approach, but perhaps aligned collagen fibers are a necessary, but not sufficient signal that leads to cell migration and cancer metastasis.

CONCLUSIONS

We demonstrated that the organization of collagen fibrils epitaxially grown on mica surfaces induces a variety of morphological and migrational behaviors depending on the specific organizational pattern of collagen. MDA-MB-231 cells that migrate using a mesenchymal mode of migration spread, elongated, oriented, and engaged in high fidelity contact guidance on the highly aligned fibrils of large width and height. As fibril organization became more random, cell orientation and contact guidance fidelity decreased. Interestingly, MTLn3 cells that migrate using an amoeboid mode of migration spread and somewhat elongated on aligned fibrils of large width and height, but did not engage in contact guidance, even though they robustly migrated. This work demonstrates that aligned collagen fibrils are a permissive, but not sufficient signal for contact guidance and that the migrational mode of different cells might impact whether a particular cell type senses directional cues such as contact guidance.

ASSOCIATED CONTENT

Supporting Information

Two figures. This material is available free of charge via the Internet at http://pubs.acs.org.

AUTHOR INFORMATION

Corresponding Author

*E-mail: ians@iastate.edu. Phone: (515) 294-0450. Fax: (515) 294-2689.

Notes

The authors declare no competing financial interest.

ACKNOWLEDGMENTS

The authors thank Carin Lightner and Ngoc Phan for protocol development and Laura Lara-Rodriguez for technical help. ICS acknowledges support from the Roy J. Carver Charitable Trust and the NIH/NCI (R03CA184575) for general project funding and from NSF ARI-R2 (CMMI 0963224) for funding the renovation of the research laboratories used for these studies. The content is solely the responsibility of the authors and does not necessarily represent the official views of the NIH. ACH acknowledges partial support by the National Science Foundation (CHE 1213582).

ABBREVIATIONS

ECM, extracellular matrix; FFT, fast Fourier transform; 3D, three-dimensional; AFM, atomic force microscopy

REFERENCES

(1) Valastyan, S.; Weinberg, R. A. Tumor metastasis: molecular insights and evolving paradigms. *Cell* **2011**, *147* (2), 275−292.
(2) Gupta, G. P.; Massague, J. Cancer metastasis: building a framework. *Cell* **2006**, *127* (4), 679−695.
(3) Petrie, R. J.; Doyle, A. D.; Yamada, K. M. Random versus directionally persistent cell migration. *Nat. Rev. Mol. Cell Biol.* **2009**, *10* (8), 538−549.
(4) Rodriguez, L. L.; Schneider, I. C. Directed cell migration in multi-cue environments. *Integr. Biol.* **2013**, *5* (11), 1306−1323.
(5) Dunn, G. A.; Heath, J. P. New hypothesis of contact guidance in tissue-cells. *Exp. Cell Res.* **1976**, *101* (1), 1−14.
(6) Guido, S.; Tranquillo, R. T. A methodology for the systematic and quantitative study of cell contact guidance in oriented collagen gels - correlation of fibroblast orientation and gel birefringence. *J. Cell Sci.* **1993**, *105*, 317−331.
(7) Wolf, K.; Muller, R.; Borgmann, S.; Brocker, E. B.; Friedl, P. Amoeboid shape change and contact guidance: T-lymphocyte crawling through fibrillar collagen is independent of matrix remodeling by MMPs and other proteases. *Blood* **2003**, *102* (9), 3262−3269.
(8) Rakic, P. Neuronal migration and contact guidance in primate telencephalon. *Postgrad. Med. J.* **1978**, *54*, 25.
(9) Provenzano, P. P.; Eliceiri, K. W.; Campbell, J. M.; Inman, D. R.; White, J. G.; Keely, P. J. Collagen reorganization at the tumor-stromal interface facilitates local invasion. *BMC Med.* **2006**, *4* (38).
(10) Ridley, A. J.; Schwartz, M. A.; Burridge, K.; Firtel, R. A.; Ginsberg, M. H.; Borisy, G.; Parsons, J. T.; Horwitz, A. R. Cell migration: Integrating signals from front to back. *Science* **2003**, *302* (5651), 1704−1709.
(11) Sabeh, F.; Shimizu-Hirota, R.; Weiss, S. J. Protease-dependent versus -independent cancer cell invasion programs: three-dimensional amoeboid movement revisited. *J. Cell Biol.* **2009**, *185* (1), 11−19.
(12) Teixeira, A. I.; Abrams, G. A.; Bertics, P. J.; Murphy, C. J.; Nealey, P. F. Epithelial contact guidance on well-defined micro- and nanostructured substrates. *J. Cell Sci.* **2003**, *116* (10), 1881−1892.
(13) Hamilton, D. W.; Oates, C. J.; Hasanzadeh, A.; Mittler, S. Migration of periodontal ligament fibroblasts on nanometric topo-

DOI: 10.1021/la503254x
Langmuir 2015, 31, 307−314

graphical patterns: influence of filopodia and focal adhesions on contact guidance. *PLoS One* **2010**, *5* (12).
(14) Meyle, J.; Gultig, K.; Brich, M.; Hammerle, H.; Nisch, W. Contact guidance of fibroblasts on biomaterial surfaces. *J. Mater. Sci.: Mater. Med.* **1994**, *5* (6-7), 463−466.
(15) Gerecht, S.; Bettinger, C. J.; Zhang, Z.; Borenstein, J. T.; Vuniak-Novakovic, G.; Langer, R. The effect of actin disrupting agents on contact guidance of human embryonic stem cells. *Biomaterials* **2007**, *28* (28), 4068−4077.
(16) Driscoll, M. K.; Sun, X. Y.; Guven, C.; Fourkas, J. T.; Losert, W. Cellular contact guidance through dynamic sensing of nanotopography. *ACS Nano* **2014**, *8* (4), 3546−3555.
(17) Romsey, N. R.; Hou, Y.; Rodriguez, L. L.; Schneider, I. C. The number of lines a cell contacts and cell contractility drive the efficiency of contact guidance. *Cell. Mol. Bioeng.* **2014**, *7* (1), 122−135.
(18) Friedl, P.; Wolf, K. Tumour-cell invasion and migration: Diversity and escape mechanisms. *Nat. Rev. Cancer* **2003**, *3* (5), 362−374.
(19) Fackler, O. T.; Grosse, R. Cell motility through plasma membrane blebbing. *J. Cell Biol.* **2008**, *181* (6), 879−884.
(20) Petrie, R. J.; Gavara, N.; Chadwick, R. S.; Yamada, K. M. Nonpolarized signaling reveals two distinct modes of 3D cell migration. *J. Cell Biol.* **2012**, *197* (3), 439−455.
(21) Stroka, K. M.; Jiang, H. Y.; Chen, S. H.; Tong, Z. Q.; Wirtz, D.; Sun, S. X.; Konstantopoulos, K. Water permeation drives tumor cell migration in confined microenvironments. *Cell* **2014**, *157* (3), 611−623.
(22) Egeblad, M.; Rasch, M. G.; Weaver, V. M. Dynamic interplay between the collagen scaffold and tumor evolution. *Curr. Opin. Cell Biol.* **2010**, *22* (5), 697−706.
(23) Kadler, K. E.; Hill, A.; Canty-Laird, E. G. Collagen fibrillogenesis: fibronectin, integrins, and minor collagens as organizers and nucleators. *Curr. Opin. Cell Biol.* **2008**, *20* (5), 495−501.
(24) Poole, K.; Khairy, K.; Friedrichs, J.; Franz, C.; Cisneros, D. A.; Howard, J.; Mueller, D. Molecular-scale topographic cues induce the orientation and directional movement of fibroblasts on two-dimensional collagen surfaces. *J. Mol. Biol.* **2005**, *349* (2), 380−386.
(25) Provenzano, P. P.; Inman, D. R.; Eliceiri, K. W.; Trier, S. M.; Keely, P. J. Contact guidance mediated three-dimensional cell migration is regulated by rho/ROCK-dependent matrix reorganization. *Biophys. J.* **2008**, *95* (11), 5374−5384.
(26) Barocas, V. H.; Tranquillo, R. T. An anisotropic biphasic theory of tissue-equivalent mechanics: The interplay among cell traction, fibrillar network deformation, fibril alignment, and cell contact guidance. *J. Biomech. Eng.* **1997**, *119* (2), 137−145.
(27) Levental, K. R.; Yu, H. M.; Kass, L.; Lakins, J. N.; Egeblad, M.; Erler, J. T.; Fong, S. F. T.; Csiszar, K.; Giaccia, A.; Weninger, W.; Yamauchi, M.; Gasser, D. L.; Weaver, V. M. Matrix crosslinking forces tumor progression by enhancing integrin signaling. *Cell* **2009**, *139* (5), 891−906.
(28) Bettinger, C. J.; Langer, R.; Borenstein, J. T. Engineering substrate topography at the micro- and nanoscale to control cell function. *Angew. Chem., Int. Ed.* **2009**, *48* (30), 5406−5415.
(29) Matthews, J. A.; Wnek, G. E.; Simpson, D. G.; Bowlin, G. L. Electrospinning of collagen nanofibers. *Biomacromolecules* **2002**, *3* (2), 232−238.
(30) Nain, A. S.; Phillippi, J. A.; Sitti, M.; MacKrell, J.; Campbell, P. G.; Amon, C. Control of cell behavior by aligned micro/nanofibrous biomaterial scaffolds fabricated by spinneret-based tunable engineered parameters (STEP) technique. *Small* **2008**, *4* (8), 1153−1159.
(31) Cisneros, D. A.; Friedrichs, J.; Taubenberger, A.; Franz, C. M.; Muller, D. J. Creating ultrathin nanoscopic collagen matrices for biological and biotechnological applications. *Small* **2007**, *3* (6), 956−963.
(32) Ruiz, S. A.; Chen, C. S. Microcontact printing: A tool to pattern. *Soft Matter* **2007**, *3* (2), 168−177.
(33) Koster, S.; Leach, J. B.; Struth, B.; Pfohl, T.; Wong, J. Y. Visualization of flow-aligned type I collagen self-assembly in tunable pH gradients. *Langmuir* **2007**, *23* (2), 357−359.
(34) Amyot, F.; Small, A.; Boukari, H.; Sackett, D.; Elliott, J.; McDaniel, D.; Plant, A.; Gandjbakhche, A. Thin films of oriented collagen fibrils for cell motility studies. *J. Biomed. Mater. Res., Part B* **2008**, *86B* (2), 438−443.
(35) Guo, C.; Kaufman, L. J. Flow and magnetic field induced collagen alignment. *Biomaterials* **2007**, *28* (6), 1105−1114.
(36) Narayanan, B.; Gilmer, G. H.; Tao, J. H.; De Yoreo, J. J.; Ciobanu, C. V. Self-assembly of collagen on flat surfaces: the interplay of collagen-collagen and collagen-substrate interactions. *Langmuir* **2014**, *30* (5), 1343−1350.
(37) Leow, W. W.; Hwang, W. Epitaxially guided assembly of collagen layers on mica surfaces. *Langmuir* **2011**, *27* (17), 10907−10913.
(38) Cisneros, D. A.; Hung, C.; Franz, C. A.; Muller, D. J. Observing growth steps of collagen self-assembly by time-lapse high-resolution atomic force microscopy. *J. Struct. Biol.* **2006**, *154* (3), 232−245.
(39) Fang, M.; Goldstein, E. L.; Matich, E. K.; Orr, B. G.; Holl, M. M. B. Type I Collagen Self-Assembly: The Roles of Substrate and Concentration. *Langmuir* **2013**, *29* (7), 2330−2338.
(40) Loo, R. W.; Goh, M. C. Potassium ion mediated collagen microfibril assembly on mica. *Langmuir* **2008**, *24* (23), 13276−13278.
(41) Jiang, F. Z.; Horber, H.; Howard, J.; Muller, D. J. Assembly of collagen into microribbons: effects of pH and electrolytes. *J. Struct. Biol.* **2004**, *148* (3), 268−278.
(42) Sun, M.; Stetco, A.; Merschrod, E. F. Surface-templated formation of protein microfibril arrays. *Langmuir* **2008**, *24* (10), 5418−5421.
(43) Wang, L.; Guo, Y.; Li, P. C.; Song, Y. H. Anion-specific effects on the assembly of collagen layers mediated by magnesium ion on mica surface. *J. Phys. Chem. B* **2014**, *118* (2), 511−518.
(44) Kirmse, R.; Otto, H.; Ludwig, T. Interdependency of cell adhesion, force generation and extracellular proteolysis in matrix remodeling. *J. Cell Sci.* **2011**, *124* (11), 1857−1866.
(45) Lichtner, R. B.; Julian, J. A.; Glasser, S. R.; Nicolson, G. L. Characterization of cytokeratins expressed in metastatic rat mammary adenocarcinoma cells. *Cancer Res.* **1989**, *49* (1), 104−111.
(46) Holliday, D. L.; Speirs, V. Choosing the right cell line for breast cancer research. *Breast Cancer Res.* **2011**, *13* (4).
(47) Edelstein, A.; Amodaj, N.; Hoover, K.; Vale, R.; Stuurman, N. *Computer Control of Microscopes Using μManager*; John Wiley & Sons, Inc.: New York, 2010.
(48) Linderman, J. J. *Receptors: Models for binding, trafficking, and signaling*; Oxford University Press, Inc.: New York, 1993.
(49) Wyckoff, J. B.; Pinner, S. E.; Gschmeissner, S.; Condeelis, J. S.; Sahai, E. ROCK- and myosin-dependent matrix deformation enables protease-independent tumor-cell invasion in vivo. *Curr. Biol.* **2006**, *16* (15), 1515−1523.
(50) Wolf, K.; Mazo, I.; Leung, H.; Engelke, K.; von Andrian, U. H.; Deryugina, E. I.; Strongin, A. Y.; Brocker, E. B.; Friedl, P. Compensation mechanism in tumor cell migration: mesenchymal-amoeboid transition after blocking of pericellular proteolysis. *J. Cell Biol.* **2003**, *160* (2), 267−277.
(51) Bailly, M.; Yan, L.; Whitesides, G. M.; Condeelis, J. S.; Segall, J. E. Regulation of protrusion shape and adhesion to the substratum during chemotactic responses of mammalian carcinoma cells. *Exp. Cell Res.* **1998**, *241* (2), 285−299.
(52) Mierke, C. T.; Rosel, D.; Fabry, B.; Brabek, J. Contractile forces in tumor cell migration. *Eur. J. Cell Biol.* **2008**, *87* (8-9), 669−676.
(53) Kraning-Rush, C. M.; Carey, S. P.; Califano, J. P.; Smith, B. N.; Reinhart-King, C. A. The role of the cytoskeleton in cellular force generation in 2D and 3D environments. *Phys. Biol.* **2011**, *8* (1).
(54) Pankov, R.; Endo, Y.; Even-Ram, S.; Araki, M.; Clark, K.; Cukierman, E.; Matsumoto, K.; Yamada, K. M. A Rac switch regulates random versus directionally persistent cell migration. *J. Cell Biol.* **2005**, *170* (5), 793−802.

DOI: 10.1021/la503254x
Langmuir 2015, 31, 307−314